

# GHZ state generation via projected squeezed states with dephasing

**B Alexander and M Tame**

Department of Physics, SU, Stellenbosch 7600, South Africa

E-mail: byron.alexander@alumni.uct.ac.za

**Abstract.** Emerging quantum technologies rely principally on quantum phenomena such as superposition and entanglement for their unique capabilities. To this end, it is essential to develop well-defined and efficient protocols to produce and further exercise control over states of quantum bits that exhibit desired quantum mechanical traits. From a pure separable multipartite state, a control sequence, which includes rotation, spin squeezing via one-axis twisting, quantum measurement and post-selection, generates a highly entangled multipartite state, which we refer to as a Projected Squeezed (*PS*) state. Through an optimization method, we then identify parameters required to maximize the overlap fidelity of the *PS* state with the maximally entangled Greenberger-Horne-Zeilinger (*GHZ*) state. This method leads to an appreciable decrease in state preparation time of  $N$ -qubit *GHZ* states when compared to preparation through unitary evolution only. The efficiency of the *PS* state protocol is studied in non-ideal experimentally relevant settings by employing numerical methods to simulate dephasing channels.

## 1. Introduction

Multipartite entangled quantum states play a central role in quantum information and related subareas. As such, there is already an established class of applications in quantum sensing [1], quantum computing [2], quantum communication [3], quantum cryptography [4] and quantum metrology [5]. This highlights the importance of the basic quantum control theoretic task, which seeks to establish well-defined methods for producing highly entangled multipartite states from initial pure separable states. In reference [6], we proposed such a protocol for producing highly entangled *GHZ*-type states which we denote as *Projected Squeezed* states (*PS* states). Using the protocol, we are able to produce *PS* states with *GHZ* overlap fidelity  $\mathcal{F} > 0.99$ . Essential steps in the protocol include spin-squeezing [7], which generates correlations between qubits, and quantum measurement (see equation (6) in reference [6]), which requires post-selection for obtaining the desired measurement outcome.

In reference [6], we considered the ideal case without decoherence, hence our computational modelling of the protocol was restricted to the symmetric subspace (known as the Dicke-basis [8]). This subspace is no longer suitable when including decoherence, since as a consequence of decoherence the state can in a sense migrate out of the subspace. Note that the dimension of the full Hilbert state space (computational basis) scales exponentially with qubit system size ( $\sim 2^N$ ), while the dimension of the symmetric subspace spanned by the Dicke-basis has linear scaling ( $\sim N + 1$ ). Due to the resultant increased computational complexity, only systems in the approximate range  $N \leq 10$  are viable for modelling using standard computational resources.

In this work we consider a low system size example of  $N = 4$  (as opposed to the original study [6] where we considered a larger spread of system size  $N$ ). We now consider the efficacy and robustness of the protocol in experimentally relevant settings, by including decoherence using numerical methods [9]. Our focus will be on dephasing, since this has been the dominant form of decoherence [10] when utilizing trapped-ion systems for spin-squeezing (our proposed experimental setup) [11].

## 2. PS State Protocol

The  $N$ -qubit Greenberger-Horne-Zeilinger state ( $GHZ$  state) [12] reads as

$$|GHZ\rangle := \frac{|0\rangle^{\otimes N} + |1\rangle^{\otimes N}}{\sqrt{2}}. \quad (1)$$

Our protocol for producing highly entangled  $GHZ$ -type states can be summarised by the following sequential steps [6]:

**Step 1:** For an  $N$ -qubit multipartite system, we initialize to an all spin-up state

$$|\psi(0)\rangle = \underbrace{|\uparrow\rangle \otimes \cdots \otimes |\uparrow\rangle}_{N\text{-qubits}}. \quad (2)$$

**Step 2:** To form the coherent spin state  $|CS\rangle$ , we execute a  $\pi/2$ -collective  $\hat{J}_x := \frac{1}{2} \sum_{i=1}^N \hat{\sigma}_i^x$  rotation of the initial all-spin up state (2), i.e.,

$$|\psi(0)\rangle \mapsto \exp\left(-i\frac{\pi}{2}\hat{J}_x\right)|\psi(0)\rangle =: |CS\rangle, \quad (3)$$

where  $\hat{\sigma}_i^x$  is the Pauli- $\hat{x}$  spin operator acting on the  $i$ -th component of the state tensor product (see Figure 1(a)). In our analysis, we use the Husimi representation as it is more intuitive for visualizing symmetric states like the  $PS$  state (see Figure 1 and Figure 2). In principle, any phase space distribution could be used.

**Step 3:** The coherent spin state then undergoes spin-squeezing by the unitary operator

$$\hat{U}_{Sq}(\chi t) := \exp\left(-i\chi t \hat{J}_z^2\right), \quad (4)$$

where  $\hat{J}_z := \frac{1}{2} \sum_{i=1}^N \hat{\sigma}_i^z$  and  $\chi t$  denotes the squeezing magnitude (see Figure 1(b)).

**Step 4:** The squeezed coherent spin state then undergoes a  $-\pi/2$ -collective  $\hat{J}_x := \frac{1}{2} \sum_{i=1}^N \hat{\sigma}_i^x$  rotation (see Figure 1(c)), i.e.,

$$\hat{U}_{Sq}(\chi t)|CS\rangle \mapsto \exp\left(i\frac{\pi}{2}\hat{J}_x\right)\hat{U}_{Sq}(\chi t)|CS\rangle. \quad (5)$$

**Step 5:** We now execute a Gaussian quantum measurement, characterized by Kraus operators, which reads as

$$\hat{A}_c := \sum_{m=0}^N \sqrt{\Pr(N-m|c)} \sum_{\{M\}} \underbrace{|\uparrow \cdots \downarrow_{j_1} \cdots \downarrow_{j_m} \cdots \uparrow\rangle}_{N\text{-qubits}} \langle \uparrow \cdots \downarrow_{j_1} \cdots \downarrow_{j_m} \cdots \uparrow |, \quad (6)$$

where  $(\sum_{\{M\}} \cdot)$  denotes the summation over all binary permutations (of length  $N$ ) with  $m$ -spin down qubits. A modification of the Kraus measurement operators described in the

original study (equation (6) in [6]) is required, since the  $PS$  state can, as a result of the dephasing channel (see equations (10)-(12) later on), migrate out of the symmetric subspace spanned by the Dicke basis. As such, the full Hilbert space should be considered. There is some level of freedom in choosing how to distribute the projector weightings, denoted  $\sqrt{\Pr(\cdot|c)}$ , without compromising the required completeness condition of Kraus operators, i.e.,  $\int \hat{A}_c \hat{A}_c^\dagger dc = \mathbb{1}$  (see [13]). Equation (6) is a natural extension of the Kraus measurement operators (equation (6) in [6]) such that the completeness condition extends to the full Hilbert space. Additionally, we consider equation (6) as it produces favourable  $GHZ$  overlap fidelity values for  $N = 4$ , about measurement outcome  $c = 0$ . The projector weightings, in summation (6), are characterized by the Gaussian probability distribution

$$\Pr(x|c) := \frac{1}{\sqrt{2\pi\sigma^2}} \exp\left[-\frac{(x-c)^2}{2\sigma^2}\right], \quad (7)$$

where  $\{c\}_{c \in \mathbb{R}}$  denotes the set of measurement outcomes (with cardinality of the continuum). The post-measurement state is given by

$$\frac{\hat{A}_c \rho \hat{A}_c^\dagger}{\text{Tr}[\hat{A}_c^\dagger \hat{A}_c \rho]}, \quad (8)$$

for measurement outcome  $c$ , which occurs with probability  $\text{Tr}[\hat{A}_c^\dagger \hat{A}_c \rho]$  [13]. Since the quantum measurement is a stochastic process, a chosen result is post-selected. The numerical models yield optimal results for the measurement outcome value  $c = 0$  (for  $N = 4$ ).

**Step 6:** Finally, in sequence, we execute collective  $\hat{J}_x$  and  $\hat{J}_y$  rotations (by  $-\pi/7$  and  $\pi/2$  respectively for  $N = 4$ ), for the purposes of generating a  $PS$  state  $\rho_{PS}$ , which has a maximal  $GHZ$  overlap fidelity  $\mathcal{F}$  (see Figure 2). The overlap fidelity between the  $PS$  and  $GHZ$  state density operators is given by

$$\mathcal{F}(\rho_{PS}) := \left( \text{tr} \sqrt{\sqrt{\rho_{PS}} \rho_{GHZ} \sqrt{\rho_{PS}}} \right)^2, \quad (9)$$

where  $\sqrt{\cdot}$  now denotes the matrix square root.

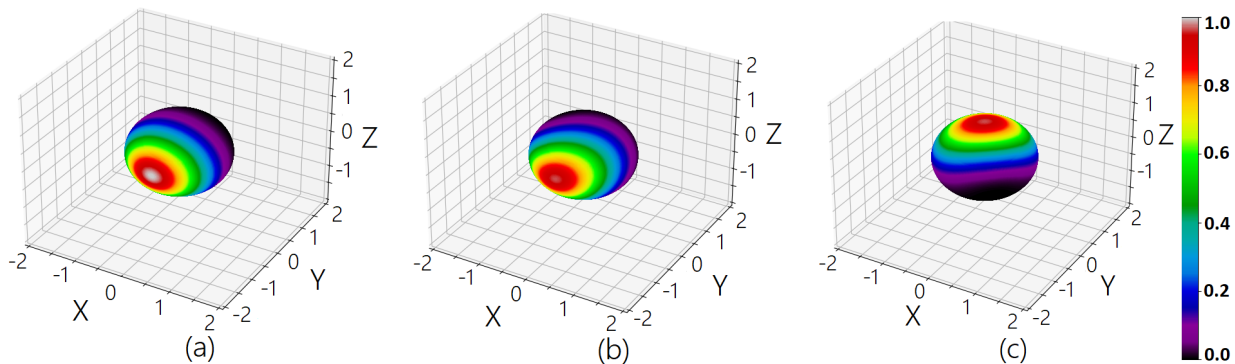


**Figure 1.** ( $N = 4$ ) Husimi representations [17] (projections onto a rotated coherent spin state) of (a) step 2 - forming the  $|CS\rangle$  state, (b) step 3 - spin squeezing by  $\chi t = .15$ , (c) step 4 - collective  $\hat{J}_x$  rotation by  $-\frac{\pi}{2}$ .

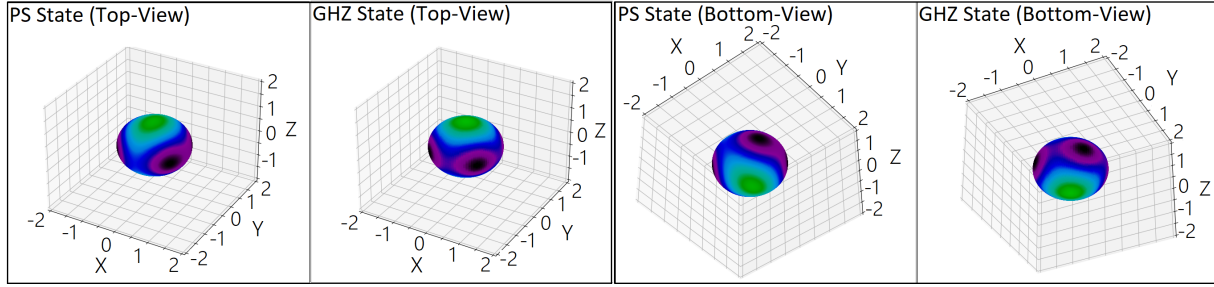


**Figure 2.** ( $N = 4$ ) Husimi representations of the *PS* state vs the *GHZ* state.

As in [6], a numerical optimization method (random walk–Markov chain Monte Carlo type regime) is employed to find, respectively, the measurement operator variance  $\sigma^2 > 0$  (see equation (7)) and squeezing magnitude  $\chi t > 0$ , which maximizes the overlap fidelity (denoted  $\mathcal{F}$ ) of the *PS* state and *GHZ* state (1). For  $N = 4$ , we find that the optimal squeezing magnitude and operator measurement variance are respectively  $\chi t = .15$  and  $\sigma^2 = 1$ .

### 3. Numerical Methods

To model the evolution of the density operator in the presence of decoherence, we utilize the (Kraus) operator sum formalism [9] given by

$$\rho(t + dt) = \sum_{\mu=0}^{\mathcal{M}} \hat{M}_{\mu}(dt) \rho(t) \hat{M}_{\mu}^{\dagger}(dt), \quad (10)$$

for infinitesimal time steps  $dt$ . For computational purposes, we approximate the infinitesimal increments  $dt$  with small finite increments hereafter denoted as  $\Delta t$ . The dephasing channels are characterized by the Kraus operators

$$\hat{M}_0 = \begin{pmatrix} \sqrt{1-p} & 0 \\ 0 & \sqrt{1-p} \end{pmatrix} \quad (11)$$

and

$$\hat{M}_1 = \begin{pmatrix} \sqrt{p} & 0 \\ 0 & -\sqrt{p} \end{pmatrix}, \quad (12)$$

with the decoherence rate given by  $\Gamma := \frac{p}{\Delta t}$ , for qubit decay probability  $p$  during time  $\Delta t$ .

The analysis which follows assumes negligible dephasing for non-squeezing steps of the protocol, whilst during the squeezing step, the dephasing operators, given by (11) and (12), act locally on each qubit. This is in line with envisioned experimental applications, utilizing ion-traps in particular [10, 11, 16]. In step 3, for finite time increments  $\Delta t$ , we interlace unitary squeezing  $\hat{U}_{Sq}(\chi \Delta t)$  with dephasing characterized by equations (10)-(12), for varied qubit decay probability values  $p = \Gamma \Delta t$ . During the squeezing step, the total dephasing time for the *PS* and *GHZ* protocols, are respectively  $n_{PS} \Delta t = .15/\chi$  and  $n_{GHZ} \Delta t = \pi/2\chi$ , where  $n_{PS}$  and  $n_{GHZ}$  are the number of  $\chi \Delta t$ -squeezing increments (for our numerical methods we assume  $\chi = 1$  and  $\Delta t = 1e^{-3}$ ). Therefore, given decay probability  $p$ , the corresponding dephasing rate is

$$\Gamma = \frac{p \chi n_{PS}}{.15} = \frac{2p \chi n_{GHZ}}{\pi}. \quad (13)$$

As in reference [6], the measurement outcome  $c \approx 0$  is post-selected (with operator variance  $\sigma^2 = 1$ ) as it yields a state with distinct probability lobes on opposing sides of the multipartite Bloch sphere (see Figure 2); this is a characteristic feature of the maximally entangled *GHZ* state (1).

#### 4. Dephasing Results

To study the efficacy of the *PS* state protocol with a given dephasing rate  $\Gamma$ , we compare it with *GHZ* state generation with  $\pi/2$ -squeezing of the coherent spin state (this yields the state  $\hat{U}_{Sq}(\pi/2)|CS\rangle$ ). This state is LU-equivalent (equivalent under local unitary operations) to the *GHZ* state (1). More specifically, a collective  $\hat{J}_x$  rotation by  $\pi/2$ , followed by a local phase gate (commonly denoted by  $S := \begin{pmatrix} 1 & 0 \\ 0 & i \end{pmatrix}$ ) acting on the  $N$ -th qubit, yields the *GHZ* state (1). As such, the unitary  $\pi/2$ -squeezing only version of the *GHZ* generation serves as a benchmark. We stress again the usefulness of the *PS* state protocol in that it requires a much shorter squeezing time compared to this benchmark, and therefore, in principle, should perform better in the presence of noise.

In Figure 3 and Figure 4, we respectively compare the quantum Fisher information (QFI) [14] (denoted by  $\mathcal{Q}(\rho, \hat{A})$  for a chosen operator  $\hat{A}$ ) with respect to the  $\hat{J}_z$  operator, and *GHZ* overlap fidelity  $\mathcal{F}$ , of the *PS* state protocol with the  $\pi/2$ -squeezing only *GHZ* state generation protocol for varying dephasing rates  $\Gamma$ .

The QFI is studied because entanglement bounds known as the *Heisenberg* and *Shot-Noise* bounds, are respectively the maximum attainable QFI (for the collective operator  $\hat{J}_z$ ), and a separable upper bound (the violation of which implies entanglement). The aforementioned Heisenberg upper bound is saturated for the *GHZ* state (hence simply labeled ‘*GHZ*’ in Figure 3). All states which violate the upper shot-noise bound are entangled [15].

As shown in Figure 3 and Figure 4, the *PS* state protocol obtains maximum QFI and *GHZ* overlap fidelity values for measurement result  $c = 0$ . From these figures, we can also observe the robustness of the protocol by noting the range of measurement outcomes for which it maintains an advantage over the *GHZ* protocol (in the presence of noise). Since the quantum measurement is a stochastic process, it is important to note that the post-selected results  $B(c = 0, 1e^{-3})$  (where  $B$  denotes an open interval, more generally an open-ball, centered about measurement result  $c = 0$ ) occur with probability  $\approx 1/20$ . This means that the improvement in preparation time is at the expense of the success probability of the protocol. Further work is needed to ascertain the trade-off between the overlap fidelity and preparation time of the *PS* state protocol and *GHZ* state squeezing only protocol.

Lastly, in Figure 4 the entanglement bound labelled ‘GME-Wit’ represents a sufficient condition (in terms of entanglement witnesses [15]) for genuine multipartite entanglement (GME). More specifically, the *GHZ* overlap fidelity  $\mathcal{F} > 1/2$  implies GME.

#### 5. Discussion

As shown in Figure 3 and Figure 4, there are experimentally relevant ranges of dephasing (see [16]), for which the reduced squeezing time of the *PS* protocol, allows the generation of states with significantly larger QFI and *GHZ*-overlap fidelity values  $\mathcal{F}$  than that generated by unitary  $\pi/2$ -squeezing only (*GHZ* protocol). The trend suggests that the *PS* state maintains an advantage for increased dephasing beyond a given qubit decay rate (for example consider  $p \in \{1e^{-3}, 1e^{-4}\}$ ).

For a larger system size  $N$ , the exponential increase in computational complexity can be suppressed by utilizing numerical methods, such as the quantum trajectory method [9]; together with computational schemes such as parallel computing. We leave the implementation of this for a future study.

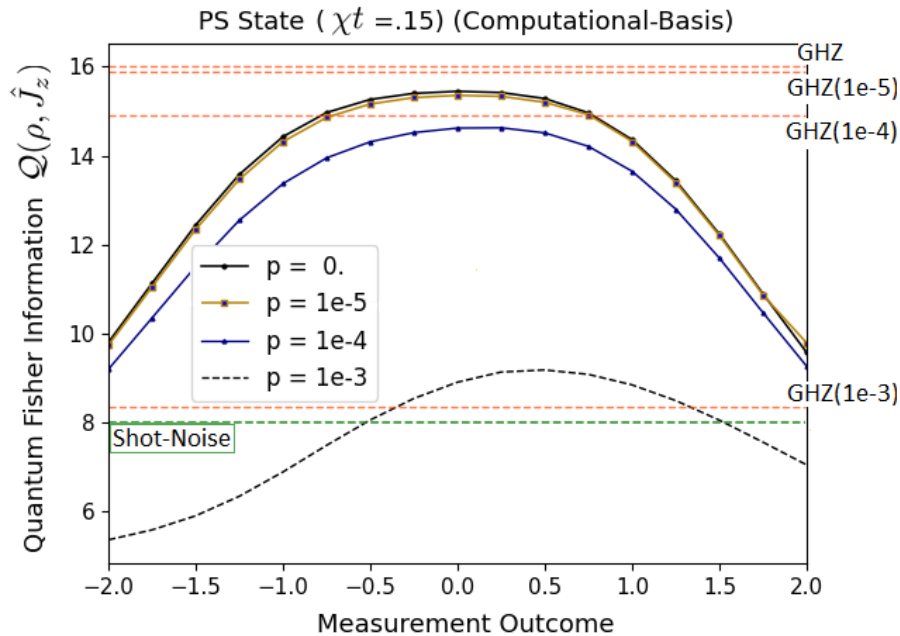


**Figure 3.** ( $N = 4$ ) QFI of the *PS* State protocol vs the squeezing only *GHZ* protocol (for varied dephasing rate  $p$ ); the latter is represented by dashed horizontal line plots (orange). The Shot-Noise upper bound (green) denotes the maximum QFI (with respect to  $\hat{J}_z$ ) for separable  $N$ -qubit systems.

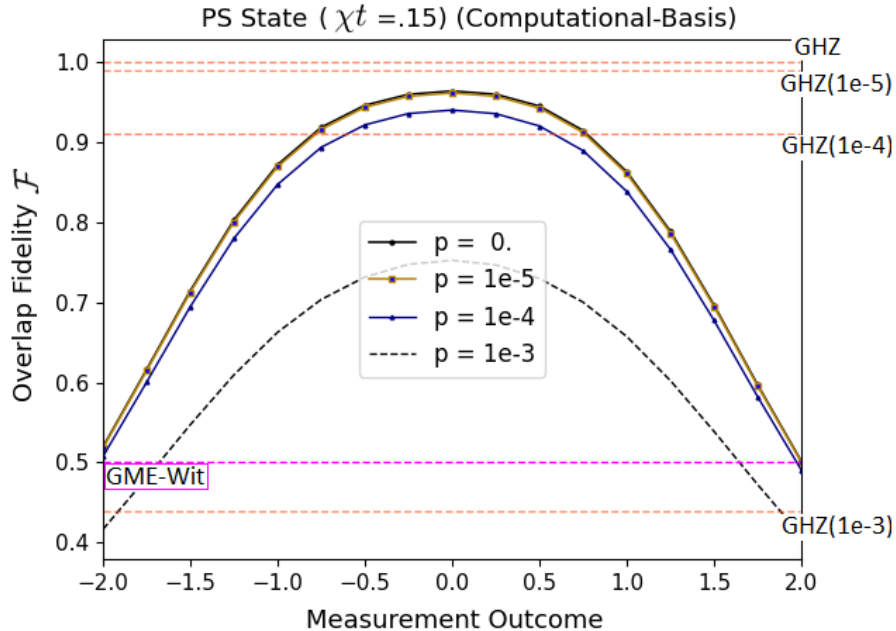


**Figure 4.** ( $N = 4$ ) Overlap fidelity of the *PS* State protocol vs the squeezing only *GHZ* protocol (for varied dephasing rate  $p$ ); the latter is represented by dashed horizontal line plots (orange). The GME-Wit lower bound (purple) denotes a sufficient condition for GME (with respect to the *GHZ* overlap fidelity  $\mathcal{F}$ ).

## Acknowledgments

We acknowledge the Council of Scientific and Industrial Research (CSIR) and the Department of Science and Technology for funding this project. Much appreciated collaborative support from the National Institute of Standards and Technology (NIST). A special note of thanks to Prof. Hermann Uys and Dr. John Bollinger for their guidance in developing the project at its inception.

## References

- [1] Degen C L, Reinhard F and Cappellaro P 2017 *Rev. Mod. Phys.* **89** 035002
- [2] Gottesman D and Chuang I L 1999 *Nature* **402** 390-93
- [3] Hillery M, Bužek V and Berthiaume A 1999 *Phys. Rev. A* **59** 1829
- [4] Jennewein T, Simon C, Weihs G, Weinfurter H and Zeilinger A 2000 *Phys. Rev. Lett.* **84** 4729
- [5] Shettell N and Markham D 2020 *Phys. Rev. Lett.* **124** 110502
- [6] Alexander B, Bollinger J J and Uys H 2020 *Phys. Rev. A* **101** 062303
- [7] Kitagawa M and Ueda M 1993 *Phys. Rev. A* **47** 5138
- [8] Dicke R H 1954 *Phys. Rev.* **93** 99
- [9] Carlo G G, Benenti G, Casati G and Mejia-Monasterio C 2004 *Phys. Rev. A* **69** 062317
- [10] Foss-Feig M, Hazzard K R, Bollinger J J and Rey A M 2013 *Phys. Rev. A* **87** 042101
- [11] Uys H, Biercuk M, Britton J and Bollinger J J 2012 *AIP Conf. Proc.* **1469** pp 108-121
- [12] Greenberger D M, Horne M A and Zeilinger A 1989 vol 37, ed Kafatos M (Dordrecht: Springer) pp 69-72
- [13] Jacobs K 2014 *Quantum Measurement Theory and its Applications* (Cambridge University Press) p 24
- [14] Tóth G and Apellaniz I 2014 *J. Phys. A* **47** 424006
- [15] Tóth G and Gühne O 2005 *Phys. Rev. A* **72** 022340
- [16] Bohnet J G, Sawyer B C, Britton J W, Wall M L, Rey A M, Foss-Feig M and Bollinger J J 2016 *Science* **352** 1297-01
- [17] Husimi K 1940 *Proc. of the Physico-Mathematical Society of Japan 3rd Series* **22** pp 264-314